Specialized Dredge Barge

Cajun Creations

Cooper Wingate, Luke Hayes, Zachary Theriot, Douglas Leonards

University of Louisiana Lafayette — Mechanical Engineering

Javeler — J.A.W.S.

PROJECT DESCRIPTION

→ The Specialized Dredge Barge is a vessel to be used for marine construction purposes that can be frequently and easily transported over land

CUSTOMER SPECIFICATIONS

→ The Barge is to be independently transportable, while remaining within regulation so that no highway permit or escort is required

→ All DOT standards must be met (weight, dimensions, lighting, etc.)

→ While in operation, the barge must support a full dredge system, including a crane, dredge pump, hydraulic power unit, and jet pump

→ The barge must have mooring capabilities and be tugboat accessible

MANUFACTURING

Water Jetting

→ Sheet metal was cut into the shape shown above through precision water jetting to allow for minimal error

Bending

→ A large metal press was used to bend the steel into the shape of the barge, eliminating manufacturing time and minimizing the potential error of the welder

Welding

→ The four corner seams were welded, and the top plate was attached via MIG welding to form a positive seal

→ All other attachments and skids for the model were welded together after precision cutting of the tubing and pipe that make up each component

FINAL DESIGN

Transportation

→ During transport, the three barges will be stacked. The load will be supported by a pinned low-bed fifth wheel hitch and a pinned rear booster axle with air suspension and lighting

Operation

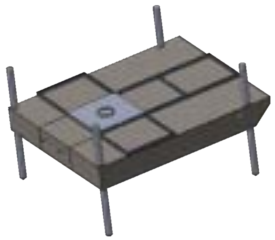

→ Barges will be connected side by side with lateral flanges for pinning

→ The barge includes two separate skids, one for mounting the crane and the other for equipment placement

→ The barge is moored with the option of 2-4 spuds

→ The front, flat face of the barges allows tugboat connections

Internal Barge Design

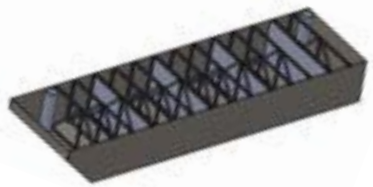

→ In the center barge, internal I-beams run across the base for connection of the front and rear attachments while adding support during transportation

→ Angle iron trusses are distributed throughout for load support during operation

→ Each hull is segmented to minimize water collection in the event of a puncture

ANALYSIS

Testing

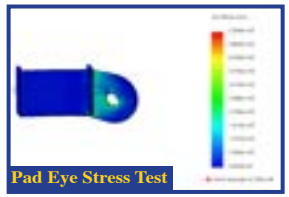

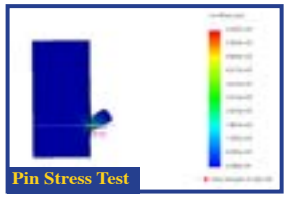

→ A Finite Element Analysis was performed via Solidworks for the beam deflection of the internal I-beams, the stress analysis on the front attachment pins, and the rear attachment connection pad eyes

Stress Equation

$$\sigma_b = (My)/I$$

σ_b - Bending Stress
M - Bending Moment
y - Centroidal Distance of the Cross Section
I – Centroidal Moment of Inertia

→ Several hand calculations were made for determining these same stresses for an assurance of the computer-aided analysis

Factor of Safety Equation

$$FOS = f_y/f_D$$

FOS - Factor of Safety
f_y - Yield Strength of Steel
f_D - Design Stress

→ A Factor of Safety was calculated to support the matching Factor of Safety from the Finite Element analysis

Buoyancy Equation

$$F_b = \rho g h A$$

F_b - Force of Buoyancy
ρ - Density of Water
g - Gravitational Constant
h - Height of the Submerged Portion of the Barge
A - Total Surface Area of the Bottom of the Barges

→ The buoyancy equation was used to determine if the barges will support the required load while the top of the barges remained the specified distance of 1.5 feet above the water line

The CAPE Foldout Array Team

CAPE-X Foldout Array

University of Louisiana at Lafayette Mechanical Engineering

Project Description

The task that the Cape Foldout Array team was given was to design a solar panel foldout array for a low orbital satellite.
Objectives:

- Fit within a 3-U CubeSat, 10x10x15cm area
- Power satellite for entirety of life cycle
- Gather data for CAPE team for future designs

All testing and data was collected in hopes to help the CAPE team build a successful low orbit satellite.

Design Criteria and Constraints

Criteria:

- Few mechanical parts
- Ease of assembly
- Survive 20Gs of acceleration forces
- Survive high temperatures
- Select materials that would not fail under these conditions
- Limit vibrations with the design
- Limit movement speed of the design
- To create as much usable surface area as possible
- Budget: $350.00

Constraints:

- Small area of storage space
- Can't interfere with electrical components
- Can't damage satellite CubeSat
- Must supply enough energy for all electrical components

The Team

Team Memebers:
Nigel Perks
Ethan Trahan
Spencer Trepagnier
Brennan Dehart

Acknowledgements: We would like to thank the following company and individuals for donating their time, materials, and expertise: Pelican Engineering for the use of the facilities, Matt Fanguy with Pelican Engineering for manufacturing parts and consulting, the CAPE Facility for access to files and resources, Dr. Paul Darby for his expertise and consulting, and Dr. William Emblom.

C.A.P.E. Cajun Advanced Picosatellite Experiment

Old Fold Out Design

In previous designs, the solar panel fold out arrays were built on the outside. This allowed for the most amount of surface space to be used for the solar panels, and the design would not get in the way of and electrical components. There are multiple different exterior designs, so the team was tasked with creating supplemental power from an interior fold out array..

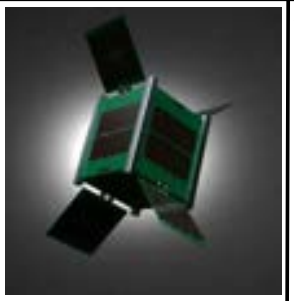

Figure 1: Cape 2 CubeSat Design

Current Design

Figure 2 Final Design

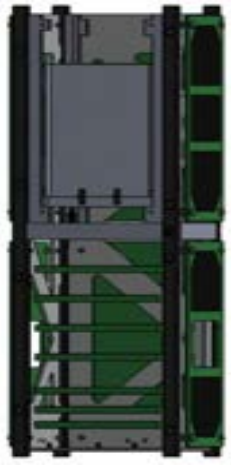

Figure 3: Cape-X Stored View

The final design that was created for this CAPE satellite involves a sled and rail system. Four panels that can have solar panels on both sides are connected to the sled and stored within the CubeSat. The sled is then connected to the railing system. While stored in the CubeSat the sled is resting on compressed spring stored in the rails. Once it reaches low orbit the springs will be released allowing for the sled to rise on the guided rail system. The panel board that are connected to the sled are connected by compression hinges and once the reach the top of the rail system they will then extend into its foldout position. This design give the most amount of surface area possible while being stored within the CubeSat. This also allows for plenty of room for the CAPE team to working inside the CubeSat without interference from the design. This design allows for most of the CubeSat to be empty because it only utilizes the walls of the CubeSat.

Analysis and Results

To begin testing this fold out array, a vibration table was created using a 12" subwoofer and car stereo. To begin, a natural frequency was determined using the material stiffness and the mass of the object. It was determined that the natural frequency was approximately 120 Hz. This data was further justified when it was put through ANSYS. To test the natural frequency using the vibration table accelerometers were attached to the sled and panel boards of the system and tested using a 40 Hz frequency on the vibration table. Using a Fast Fourier Analysis, the natural frequency that was detected was approximately 120 Hz with some harmonic frequencies elsewhere. The Fast Fourier analysis was calculated for all three axes. The final test conducted was running the full design through a vibration profile. The vibration along this profile can be seen in the figure below. As seen in the graph the vibration experienced by the design far exceeds the ideal profile, implying a change in design or vibration table may be necessary.

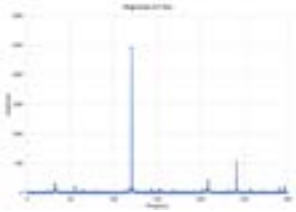

Figure 4: Y Axis FFT

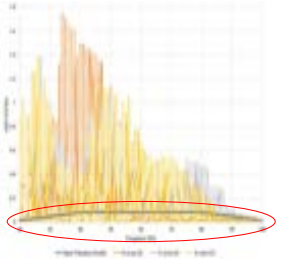

Figure 5: Vibration along Ideal Profile

Figure 6: Testing Appartus and Design

Why is this research important?

The Cape Team is currently in development of its 4th low orbit satellite and plan on building more in the future. By creating a new design and gathering data on it, this gives the team more information to use when it comes to testing and building the final design for any future satellites.

Design of a Heat Exchanger and Water Capture System to Eliminate Contrails

Kane Bergeron
ULL Mechanical Engineering
Team Leader

Ricky Swaim
ULL Mechanical Engineering
CAD and CFD Analysis Lead

Diego Sanchez
ULL Mechanical Engineering
Project Timeline Coordinator

Brett Weber
ULL Mechanical Engineering
Testing Coordinator

Introduction

Aviation is a vastly growing industry and with it so does its effects on the atmosphere. In order to reduce aviation's global effect, the best place to start would be contrails. This is because the number one source of global effects resulting from the use of aircrafts is contrails. One method that has been researched is the use of a fuel source with a cleaner exhaust like that of a Solid Oxide Fuel Cell (SOFC).

- Objective: Create a low drag design for a heat exchanger and water capture system that will eliminate aircraft contrails when used in conjuction with a SOFC system

Background Information

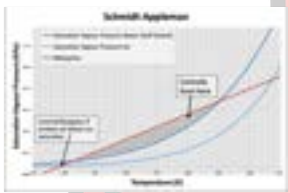

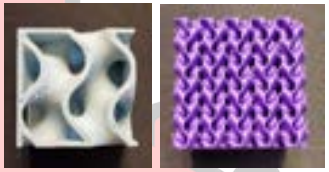

Gyroid TPMS Structure

- Contrail avoidance is dependent upon air saturation and the conditions at which plane exhaust and the atmosphere mixes
- TPMS structure formed through combination of sines and cosines
- Additive manufacturing can produce complex geometries, thinner features, and up to a 15% increase in heat transfer
- NACA ducts provide a low drag option for inlet due to their overall structure and embedment into the plane structure

Material Selection Data

Material	Fatigue Limit	Thermal Conductivity	Density	Melting Point
Titanium Ti-6Al-4V	680 MPa	6.70 W/m-K	4.41 g/cc	1604-1660°C
6061 Aluminum	62.1 MPa	180 W/m-K	2.70 g/cc	582-651.7°C
Silver	90 MPa	419 W/m-K	10.491 g/cc	961.93 °C
Pure Copper	150 MPa	357 W/m-K	8.93 g/cc	1083.2-1083.6°C

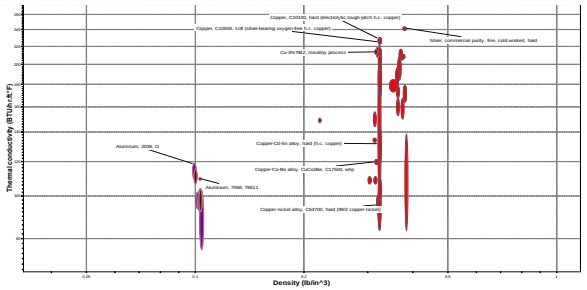

Ashby Plot of Thermal Conductivity vs Density

Assumptions and Calculations

Assumptions for CFD Analysis

Fluid Designation	Pressure (atm)	Inlet Temp (K)	Heat Transfer Coefficient (W/m^2*K)	Mass Flow (g/s)
Atmospheric	0.22	217	5-10	1745
Exhaust	0.22	547	5-10	1100

Material for CFD Analysis

Material	Thermal Conductivity (W/m*K)	Density (kg/m^3)	Thickness (mm)	Surface Area (m^2)
Copper Alloy	370	8930	5.08	25.66

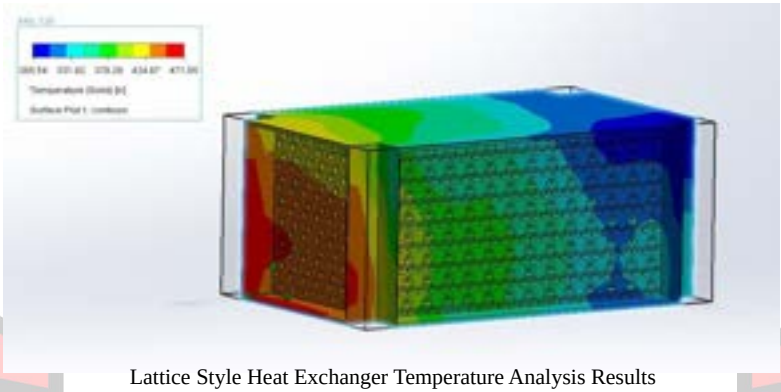

Lattice Style Heat Exchanger Temperature Analysis Results

Overall System Design

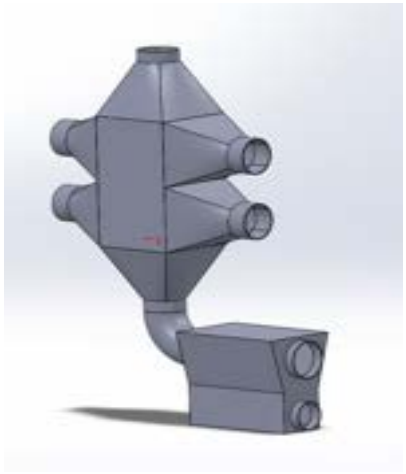

Overall System Design

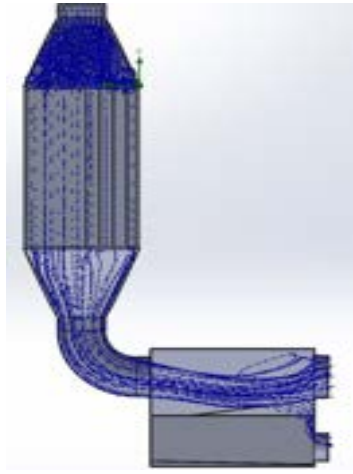

Overall System Flow Patterns

Analysis Results

CFD Analysis Results

Fluid Designation	Pressure (atm)	Outlet Temp (K)	Mass Flow (g/s)	Heat Transfer (kW)
Atmospheric	0.22	217	1745	323.5
Exhaust	0.22	547	1100	323.5

Recommendations

- Heat Exchanger – Lattice Style Heat Exchanger
- Cell Shape – Gyroid structure w/ defining equation
  $\sin(x)\cos(y) + \sin(y)\cos(z) + \sin(z)\cos(x)$
- Material – Copper Alloy (Cu-3%TiB2 – Copper Titanium Boride)
- Material Thickness – Minimum thickness required 0.0104 in.
  Designed thickness to be used 0.2 in.
- Manufacturing Process – Additive manufacturing
  (Selective Laser Melting)
- Inlet – NACA ducts for minimal drag used in conjunction with variable flow device

Conclusions

- In order to avoid contrails, maximum water separation and pullout needs to occur as well as an elevated exit temp
- A Lattice Style Heat Exchanger provides the lightest, most compact, and highest functioning option
- A Copper Alloy will provide the best compromise between weight and heat transfer
- NACA ducts should provide a minimal amount of drag
- CFD analysis showed temperature in heat exchanger would reach dew point, .
- Calculations showed structure able to withstand maximum compressive force of 560 lbf and the needed pressure of 300 psi

References

[1] Rajashekara, Kaushik, et al. "Solid Oxide Fuel Cell/Gas Turbine Hybrid APU Systemfor Aerospace Applications." Conference Record of the 2006 IEEE Industry ApplicationsConference Forty-First IAS Annual Meeting, 2006, doi:10.1109/ias.2006.256845.

[2] F. Noppel and R. Singh. Overview on Contrail and Cirrus Cloud Avoidance Technology.Journal of Aircraft, 44(5):1721-1726, October 2007.

[3] Whelan, Gillian & Cawkwell, Fiona & Mannstein, Hermann & Minnis, Patrick. (2009). The use of Meteorological Data to Improve Contrail Detection in Thermal Imagery over Ireland.

[4] Saltzman, David, et al. "Design and Evaluation of an Additively Manufactured Aircraft Heat Exchanger." *Applied Thermal Engineering*, vol. 138, 2018, pp. 254–263., doi:10.1016/j.applthermaleng.2018.04.032.

[5] "Online Materials Information Resource." MatWeb, www.matweb.com/.

Design of a Heat Exchanger and Water Capture System to Eliminate Contrails

Kane Bergeron
ULL Mechanical Engineering
Team Leader

Ricky Swaim
ULL Mechanical Engineering
CAD and CFD Analysis Lead

Diego Sanchez
ULL Mechanical Engineering
Project Timeline Coordinator

Brett Weber
ULL Mechanical Engineering
Testing Coordinator

Introduction

Aviation is a vastly growing industry and with it so does its effects on the atmosphere. In order to reduce aviation's global effect, the best place to start would be contrails. This is because the number one source of global effects resulting from the use of aircrafts is contrails. One method that has been researched is the use of a fuel source with a cleaner exhaust like that of a Solid Oxide Fuel Cell (SOFC).

- Objective: Create a low drag design for a heat exchanger and water capture system that will eliminate aircraft contrails when used in conjuction with a SOFC system

Background Information

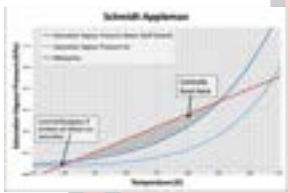

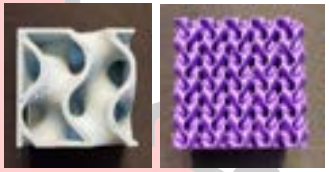

Gyroid TPMS Structure

- Contrail avoidance is dependent upon air saturation and the conditions at which plane exhaust and the atmosphere mixes
- TPMS structure formed through combination of sines and cosines
- Additive manufacturing can produce complex geometries, thinner features, and up to a 15% increase in heat transfer
- NACA ducts provide a low drag option for inlet due to their overall structure and embedment into the plane structure

Material Selection Data

Material	Fatigue Limit	Thermal Conductivity	Density	Melting Point
Titanium Ti-6Al-4V	680 MPa	6.70 W/m-K	4.41 g/cc	1604-1660°C
6061 Aluminum	62.1 MPa	180 W/m-K	2.70 g/cc	582-651.7°C
Silver	90 MPa	419 W/m-K	10.491 g/cc	961.93 °C
Pure Copper	150 MPa	357 W/m-K	8.93 g/cc	1083.2-1083.6°C

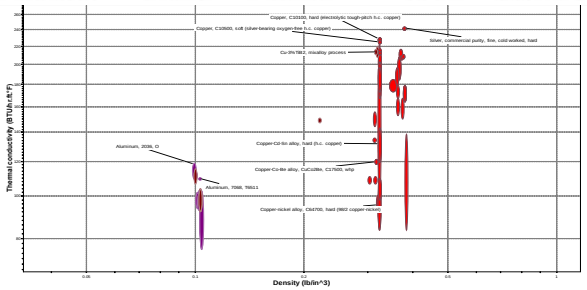

Ashby Plot of Thermal Conductivity vs Density

Assumptions and Calculations

Assumptions for CFD Analysis

Fluid Designation	Pressure (atm)	Inlet Temp (K)	Heat Transfer Coefficient (W/m^2*K)	Mass Flow (g/s)
Atmospheric	0.22	217	5-10	1745
Exhaust	0.22	547	5-10	1100

Material for CFD Analysis

Material	Thermal Conductivity (W/m*K)	Density (kg/m^3)	Thickness (mm)	Surface Area (m^2)
Copper Alloy	370	8930	5.08	25.66

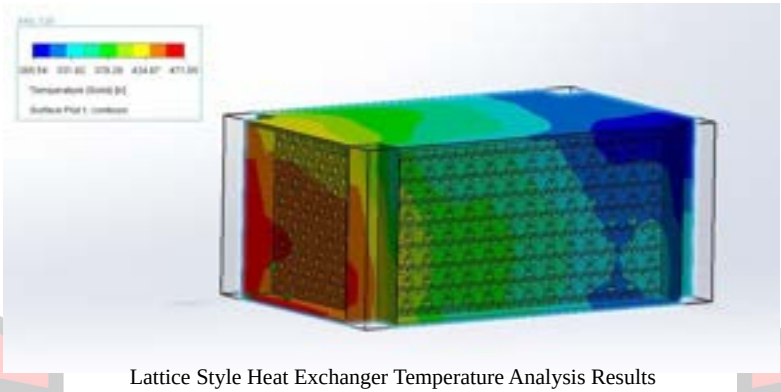

Lattice Style Heat Exchanger Temperature Analysis Results

Overall System Design

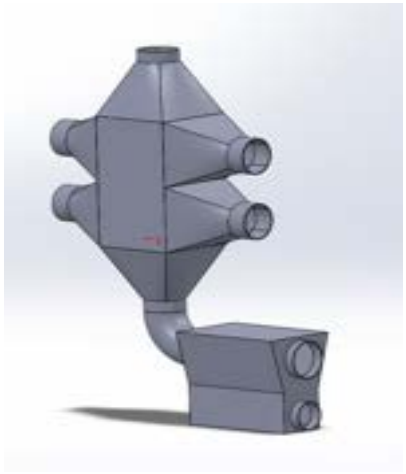

Overall System Design

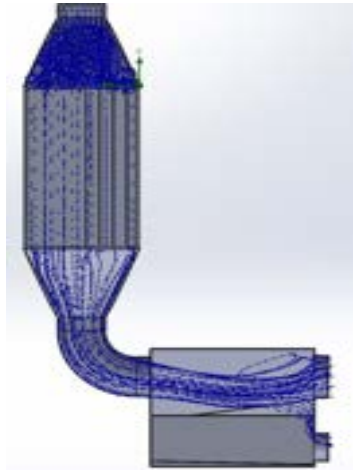

Overall System Flow Patterns

Analysis Results

CFD Analysis Results

Fluid Designation	Pressure (atm)	Outlet Temp (K)	Mass Flow (g/s)	Heat Transfer (kW)
Atmospheric	0.22	217	1745	323.5
Exhaust	0.22	547	1100	323.5

Recommendations

- Heat Exchanger – Lattice Style Heat Exchanger
- Cell Shape – Gyroid structure w/ defining equation
  $\sin(x)\cos(y) + \sin(y)\cos(z) + \sin(z)\cos(x)$
- Material – Copper Alloy (Cu-3%TiB2 – Copper Titanium Boride)
- Material Thickness – Minimum thickness required 0.0104 in.
  Designed thickness to be used 0.2 in.
- Manufacturing Process – Additive manufacturing
  (Selective Laser Melting)
- Inlet – NACA ducts for minimal drag used in conjunction with variable flow device

Conclusions

- In order to avoid contrails, maximum water separation and pullout needs to occur as well as an elevated exit temp
- A Lattice Style Heat Exchanger provides the lightest, most compact, and highest functioning option
- A Copper Alloy will provide the best compromise between weight and heat transfer
- NACA ducts should provide a minimal amount of drag
- CFD analysis showed temperature in heat exchanger would reach dew point, .
- Calculations showed structure able to withstand maximum compressive force of 560 lbf and the needed pressure of 300 psi

References

[1] Rajashekara, Kaushik, et al. "Solid Oxide Fuel Cell/Gas Turbine Hybrid APU Systemfor Aerospace Applications." Conference Record of the 2006 IEEE Industry ApplicationsConference Forty-First IAS Annual Meeting, 2006, doi:10.1109/ias.2006.256845.

[2] F. Noppel and R. Singh. Overview on Contrail and Cirrus Cloud Avoidance Technology.Journal of Aircraft, 44(5):1721-1726, October 2007.

[3] Whelan, Gillian & Cawkwell, Fiona & Mannstein, Hermann & Minnis, Patrick. (2009). The use of Meteorological Data to Improve Contrail Detection in Thermal Imagery over Ireland.

[4] Saltzman, David, et al. "Design and Evaluation of an Additively Manufactured Aircraft Heat Exchanger." *Applied Thermal Engineering*, vol. 138, 2018, pp. 254–263., doi:10.1016/j.applthermaleng.2018.04.032.

[5] "Online Materials Information Resource." MatWeb, www.matweb.com/.

NFPA Fluid Power Vehicle Challenge

John Parker Furman, Tristan Jeansonne, Jacob Laberteaux, Christopher Bertrand
Yasmeen Qudsi and Aaron Darnell

Introduction

The National Fluid Power Association created the Fluid Power Vehicle Challenge to inspire students to explore fluid power and to provide networking opportunities within the fluid power industry. The FPVC consists of three challenges: a 500 foot Sprint Race, a half-mile Endurance Challenge with regenerative braking, and an Efficiency Challenge [1]. Teams are allowed to continue working on vehicles from previous years. As a first year team, this meant building an entire vehicle instead of enhancing a subsystem.

Objectives

The primary objective was to create a safe, functional vehicle that would be able to participate in the competition. Other objectives were to do well in the Efficiency Challenge, remain within budget, expand UL's reputation in the fluid power industry, and leave a good starting point for future UL teams.

Sizing Components

The NFPA provided a series of equations to the teams to properly size the hydraulic parts that would be needed [2]. It was calculated that a 0.513 CID motor and a 0.580 CID pump would be used.

Table 1: Sizing Results

Max Pull	10.5 lbs	Pump RPM	240 RPM
Torque	136.44 lbs*in	Pump CID	0.458 CID
Motor CID	0.429 CID	Pump Size	0.509 CID
Motor Size	0.476 CID	GPM Required	0.431 GPM
Wheel RPM	194 RPM	Hose Diameter	0.188 in

Final Vehicle

Figure 1: Final Design of Vehicle on Competition Day

The final design of the bike weighed 125 pounds and met all specifications required by the competition. Stabilizing wheels were added to increase stability and safety. The hydraulic circuit is behind the rider on the added platform. The pneumatic and electronic subsystems are attached in front of the rider on the handlebars.

Hydraulic Circuit

The hydraulic control circuit utilizes a pump and an accumulator to direct fluid through a system of valves and a motor to create fluid power. The system can perform four different drive modes including Direct Drive, Accumulator Charge, Accumulator Drive, and Regenerative Braking.

Figure 2: Hydraulic Circuit

Pneumatic Brake

The vehicle's front brake was modified into a pneumatic brake. The pneumatic brake uses a single acting cylinder to engage the front brake pads on the wheel. A reservoir is used to store compressed air, a regulator is used to regulate the pressure, and a three way valve is used to allow air into the cylinder and allow air out of the system.

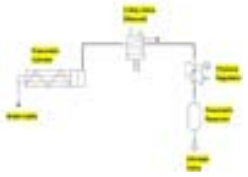

Figure 3: Pneumatic Circuit

Electronic Controls

The solenoid values of the hydraulic circuit are controlled by electronics stored on the handlebars of the vehicle. Toggle switches activate relays that power the solenoid values from a 12V drill battery. Each switch is labeled on a chart with the configurations of each mode. This chart was placed on top of the enclosure for easy viewing.

Figure 4: Electronics Enclosure

Results

The bike performed as expected from simulation. The top speed was 11mph with a Sprint Race time of 44.1 seconds. The efficiency was 10%. These results and other competition events led to Team Hydro placing

- 3rd in the Sprint Race
- 1st in the Efficiency Challenge
- 3rd Overall

For this Team Hydro was awarded $2,000.

Conclusion

Placing 3rd Overall as a first year team, Team Hydro left a good impression on the NFPA for UL, and future teams will have a working starting point to build upon in future competitions.

References

[1] "Overview, Rules, and Awards," *NFPA Fluid Power Vehicle Challenge*. https://fpvc.secure-platform.com.

[2] "Educational Webinar on Sizing Components and Conductors." https://www.youtube.com/watch?v=Zc0xi-SGRtY.

FSE Team

Friction Stir Extrusion Machine

University of Louisiana Lafayette Mechanical Engineering

Project Description

A friction Stir Extrusion Machine uses a high angular velocity probe moving through the workpiece in order to form the material into a desired shape. There are two types of extrusions: Forward and Back Extrusion. The FSE Team was given the task of successfully back extruding, using a dome tipped tooling to produce a hollow aluminum workpiece. The FSE Team was also responsible for doing so, with the machine being fully automated, using a Programmable Logic Controller, or PLC, to control the movements of the machine.

Design Criteria and Constraints

Criteria:

- Fully automated
- Back Extrude a ½ inch aluminum workpiece
- Limit vibrations
- Remain under a $500 budget
- Ensure the machine is safe for the user
- Simplicity when operating

Concerns:

- A plunge force when forward extruding a 1 ½ inch diameter being too large for the screw jack
- Difficulty In machining a coupler to connect the gearbox to the screw jack
- Having the aluminum workpiece get welded and stuck to the tooling

Meet The Team

Pictured here is the full FSE team. Starting from left to right, is Electrical Engineers Dylan Bordelon and Charles Kreamer. Next Is Mechanical Engineers Ross Foreman, Michael Leaumont, Sydney Frazier, and Seth Doiga.

Acknowledgements:
On behalf of the mechanical design team, we would like to acknowledge the former mechanical teams responsible for the machine frame as well as the electrical team for their much-needed contributions. Lastly, we express an appreciation to our sponsor, Professor Emblom, for funding the project and providing help and encouragement along the way.

The Design

The FSE Team's focus over the goal of the project was to replace a manual hand crank, used to raise and lower the die plate, and replace it with a stepper motor connected to the screw jack for automated control. The TRIZ Diagram shown in Figure 1, displays how the project was divided into multiple parts: the machine frame, extrusion tooling and die, automation of operation, and the electronic components. Upon further calculation analysis, the team decided to transition from forward extrusion to back extrusion. This required for the machining of a new die. Figure 2 shows an updated model of the current die body the FSE team is using to perform test through back extrusion.

Figure 1: TRIZ Diagram

Figure 2: New Die Model

Figure 3: Final Design

Figure 4: Final Assembly

The Final Design consist of a stepper motor, coupler, and gearbox to produce vertical, automated movement of the die plate. On the left of the machine, two rails were added in order to mount the NEMA box. This box holds and protects the electronics being used for automation. These include the Programmable Logic Controller and the Variable Frequency Drive. To ensure safety when operating, a distance sensor was mounted to the machine. The die plate would slowly rise to the limit set by the operator, hitting the button on the distance sensor, then killing power to the machine.

Analysis and Results

The FSE Team went through multiple rounds of testing throughout the semester. Due to a complication in parts, most of the test were ran using the manual hand crank to raise and lower the die plate. The goal of the test being portrayed was to extrude an aluminum sample with a constant extrusion force of 150lbs of force. This test included a low-force time period of 60 seconds to allow the aluminum sample to preheat prior to extrusion.

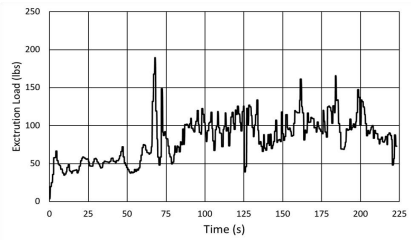

Figure 5: Time vs. Extrusion Load

Figure 5 shows the time of the test compared to the Extrusion Load. The steady reading of around 50lbs for the first 60 seconds shows the initial warm up period for the workpiece. After 60 seconds, the target force for the hand crank operator was increased to 100lbs. The target load of 100lbs allowed for the FSE team to successfully extrude the aluminum workpiece at a constant force.

Figure 6: Extruded Workpiece

Figure 7: Before and After Extrusion

Figure 6 and 7 show the results of a successful back extrusion. Using a spindle speed of 3000 RPM, there was a significant decrease in vibrations of the guide rails and die table, ensuring a constant extrusion. The FSE team was able to successfully extrude 37.9mm into the aluminum workpiece.

Why is this research important?

Friction Stir Welding was first invented in 1991 by Wayne Thomas at the Welding Institute in Cambridge, UK. Friction Extrusion can be used to form fully consolidated wires, rods, and tubes. Friction Extrusion is used in applications such as aerospace and automotive manufacturing.

C.R.A.W.LAB
http://www.ucs.louisiana.edu/~jev9637/

RoboBoat 2.0 with a UAV

Brennan Moeller, Nathan Madsen, Joseph Stevens, Benjamin Willis
Advisors: Dr. Joshua Vaughan and Yasmeen Qudsi

University of Louisiana Lafayette — Mechanical Engineering

Project Overview

This project's goal was to design and integrate an Unmanned Aerial Vehicle (UAV) to act as an autonomous, mobile sensor to aid an Autonomous Surface Vessel (ASV) in data collection for navigating the 2021 RoboBoat competition in late May. RoboBoat is a competition where students are tasked to design and build an ASV to autonomously navigate through various tasks in a marine environment. The general course layout is shown in Figure 1. In 2019, a ULL RoboBoat team designed and built the initial version of the ASV.

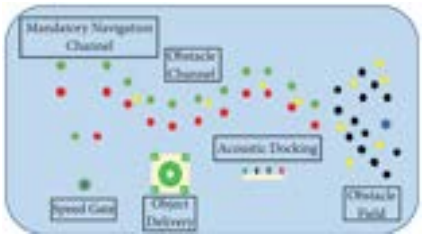

Figure 1: 2021 RoboBoat Competition Course [1]

2019 UL Lafayette ASV

The proposed system is to be integrated with the 2019 ULL ASV that is shown in Figure 2. The ASV displayed below is running the Robot Operating System (ROS) on its on-board computers. ROS is an open source framework that aids in the control, implementation of algorithms, and communication between robots. ROS also aids in the integration of multi-agent robotic systems by allowing collected information to be shared across multiple systems.

Figure 2: 2019 UL Lafayette ASV

Final Design

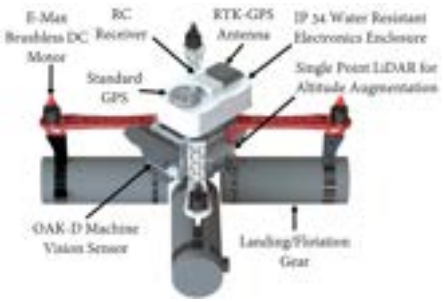

Figure 3: Main ASV System

Figure 4: Multi-agent System

Component Design

Buoyancy

Figure 5: It Floats!

Figure 6: Underwater View

Buoyancy Calculations	
Parameter	Value
Total Weight (lbs)	4.23
Submerged Volume of Landing Gear (in^3)	240
Buoyancy Force (lbs)	5.43

Thrust

Thrust to Weight Ratio	
Parameter	Value
Desired Thrust to Weight Ratio	2:1
Actual Thrust to Weight Ratio	1.8:1

Thrust to Weight Ratio Improvements		
Parameter	PCB	Carbon Fiber
Top Plate (lbs)	0.06	0.05
Bottom Plate (lbs)	0.09	0.06

Center of Mass

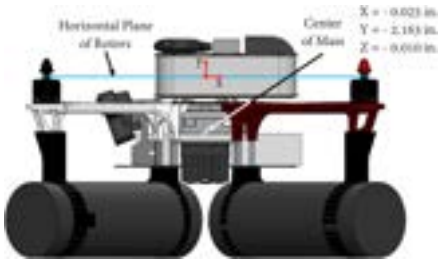

Figure 7: UAV Center of Mass

The location of the center of mass, in reference to the plane in which the rotors lie, determines the UAV's stability during forward flight and its ability to combat wind disturbances.

Global Positioning Requirements

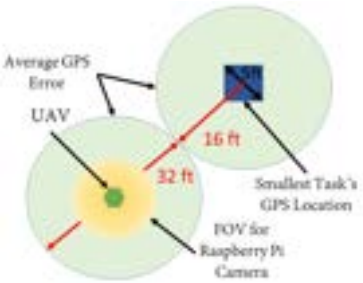

Figure 8: GPS Error Analysis

This GPS error drove the need for a Real-Time Kinematic (RTK) global positioning system.

Acknowledgements

Hammond Manufacturing and AWC, Inc. for their generous donation of the new electronics enclosure.

Chapman Consulting Inc. for their generosity in allowing us access their facilities and resources.

OpenCV, Luxonis, and Intel for sponsoring the OAK-D AI Competition.

References

[1] RoboNation RoboBoat.
Roboboat-2021-rules-and-task-description$_{2}$2, 2021.

The Cajun Concentrator

CPV21 Team

University of Louisiana at Lafayette — Mechanical Engineering

Project Description

- Concentrated solar power is a technology of untapped potential, yielding large outputs, but are largely inefficient.
- Photovoltaic cells provide energy but require a large surface area to be cost and production effective.
- Project scope is to design and fabricate a prototype Conical Dish Receiver (CDR) with a Concentrated Photovoltaic (CPV) target testing system to autonomously track the sun's path and produce increased electrical energy.
- This device will allow for further research to be conducted on concentrated photovoltaic energy generation

Design Criteria and Constraints

Criteria:

- Must utilize a Conical Dish Receiver
- Must utilize photovoltaic cells to generate power
- Must follow sun path autonomously (dual axis tracking mechanism)
- Provide system output of 1,650W
- Include active and/or passive cooling to minimize power loss
- Provide AC Signal generation
- Integrate necessary safety features
- System is preferably mobile and collapsible
- Construct within cost limitations (budget: $12,500)

Constraints:

- Weight/size/geometry
- Adequate alignment for concentration tolerance in fabrication
- PV cell properties
- Heat generated in concentration
- Programming a control system to precisely track the sun

The Team

CPV21 Team:
(left to right)
Dr. Kary Ritter,
Zachary Parks,
Noah Pontiff,
William Galtier,
Benjamin Tauzin,
Robert Bentley, and
Dr. Terrance Chambers

Acknowledgments:
The design team would like to thank our industry sponsor Mr. Glenn Reynolds with Gossamer Space Frames, LLC as well as faculty sponsors Dr. Chambers and Dr. Ritter.
Also, a special thanks to Mr. Robert Bentley, Ms. Yasmeen Qudsi, Mr. Jeff Guidry, and Mr. Dana Patin for extensive fabrication support.

The Design

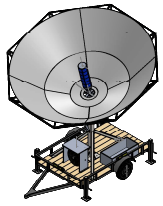

Preliminary Cajun Concentrator Mk. I Model

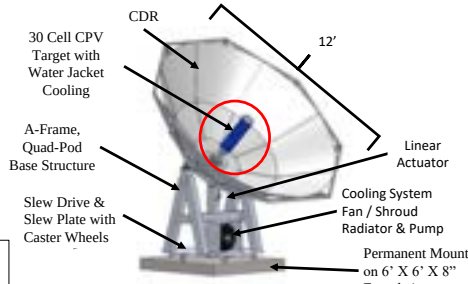

Cajun Concentrator Mk. II Model

How It Works:

Structural shortcomings of preliminary design led to development of the Cajun Concentrator Mk II. This machine consists of a 4-tier reflective mirror sheet CDR with a central cylindrical 30 cell CPV target. The water jacket cooling system within the target paired with a pump/radiator and fan removes heat from the cells. Dual axis sun tracking is achieved with a 1,000 lbf linear actuator for tilt (elevation) and 1,500 ft-lb slew drive for rotary motion (azimuth). Automation is controlled with an Arduino board conjoined with a Campbell Scientific data logger programed to track following NREL sun path data.

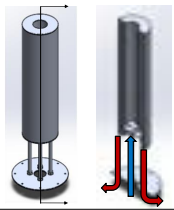

CPV Target Water Jacket

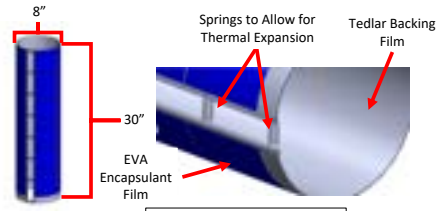

CPV Target Sleeve

Validating the Design:

- Light reflection physics was applied using the 2-alpha angle principle to derive necessary conical tier concentration angles.
- Heat transfer analysis of the CPV Target water jacket cooling system yields and expected cell surface temperature of around 74° F
- Theoretical output calculations and experimentation were used to determine the maximum expected power output of 2,160 W

Analysis and Results

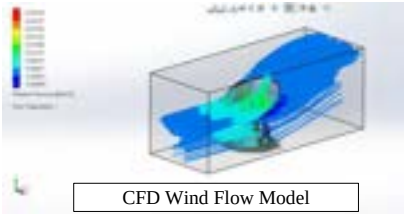

CFD Wind Flow Model

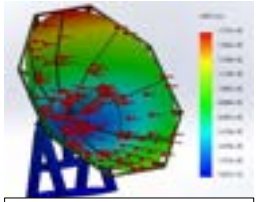

FEA Wind Load Simulation

SolidWorks simulations were conducted to ensure the structural integrity of the design under wind loading. Tier angles and concentration ratio were derived with the 2α light reflection principle and the surface area ratio between the CDR aperture and cylindrical target surface. Heat transfer and pressure calculations were developed to validate theoretical function of the water-jacket active CPV cooling system. Bolt and weld analysis were computed with machine design calculations to ensure strength at all joints.

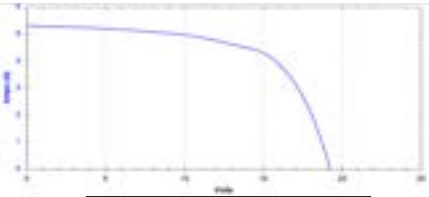

Baseline IV Curve Test

Concentrated output was measured at 150W. This more than doubled the baseline output, however the CPV panel sleeve was destroyed by the concentrated heat.

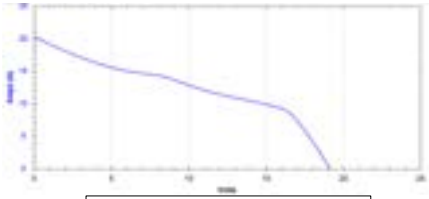

Concentrated IV Curve Test

CPV Panel Sleeve Post-Concentration

Future Design Improvements:

- Improve the CPV Target with incorporation of better suited PV cells.
- Improve the CDR reflective sheet alignment methods
- Develop more accurate automated sun tracking methods
- Utilize brackets and pins to replace welds for DFMA principles
- Improve Cooling System heat transfer to reduce efficiency drop
- Incorporate device mobility and further collapsibility

Importance of This Research

The Cajun Concentrator constructed during the pioneer CPV/CDR Solar Collector Project shall function as a ULL test bed for research and developments surrounding this technology. This concept has potential for mass commercial production due to significantly higher efficiencies that may be achieved through combined PV and solar-thermal power production. Exciting possible applications range from residential power supply to hydrogen production.

Micro-Tube Hydroforming

Fall 2021 MCHE Team

Connor Frederick, Kenneth Earles III, Collin Taylor, Grant Carline

Advisor: William J. Emblom, Ph.D

Special Thanks to Our Sponsors:

TUBE HYDROFORMING PROCESS

Micro-tube hydroforming is a process by which tubes of various materials are subjected to high internal pressures by an incompressible fluid and used to permanently deform the material. This process is achieved by clamping the tube inside of a two-part die cavity, pressurizing, and allowing the tube to deform along ideal loading curves into a desired geometry.

PROJECT BACKGROUND INFORMATION

Tube hydroforming (THF) is a well-known manufacturing process for easily & efficiently producing parts such as T-joint fittings, automotive chassis, & bicycle frames. THF on a micro scale has not yet been implemented in industry, and has only been accomplished by a handful of groups. The ultimate goal of the micro-THF project at ULL is to develop a THF system capable of hydroforming 2mm OD steel tubing into T-joint fittings. Achievement of this goal will open up avenues of research and development in the realm of micro-manufacturing.

CURRENT PROJECT SCOPE

The scope of the 2021 MCHE & EE teams is to develop a PLC controlled micro-tube ***bursting*** system. Completion of the current scope will frame the system for future modifications in order to hydroform micro-tubes into more complex geometries. Objectives of the current scope are as follows:

- ➔ PLC controlled hydraulic pump & linear actuators.
- ➔ Programmed safety measures in the case of material failure.
- ➔ Data acquisition of testing time, actuator displacement & force, & pressure.
- ➔ Tooling manufacturing & assembly.
- ➔ Tube burst testing, results analysis, & suggestions for essential modifications.

TOOLING DESIGN PROCESS

A tooling system capable of pressurizing micro-tubes to burst was developed to operate in conjunction with an Allen-Bradley Micro820 PLC. The most important & difficult design factor considered is the tooling alignment. Concentricity of each tooling component is key to sealing the microscale tube-faces against pressures up to 35 KSI.

In order to achieve ultra-accurate alignment within the tolerance of 0.4mm, the following components & techniques were implemented:

- ➔ A linear plain bearing pillow-block
- ➔ A custom CNC machined actuator coupler machined to a tolerance of +0.0”/-0.0008” to achieve an ANSI RC3, precision-running fit within the linear bearing.
- ➔ An surface finish of 7.5 RMS on the actuator coupler.
- ➔ 3D-printed lift blocks for vertical concentricity of tooling components.
- ➔ Self-aligning hemispherical sealing inserts.
- ➔ PTFE thread tape applied between the sealing inserts and the crimped tube ends to achieve sealing against pressures of up to 35 KSI.
- ➔ Meticulous tooling component assembly.
- ➔ Validation testing of each component upon installation.

FINAL TOOLING DESIGN

TESTING PREPARATION PROCEDURE

Creating a useful tube sample for the micro-THF system is a multi-stage process which are conducted in the following order:

1. Cutting tubes to a length of 75mm with a dremel cutting blade.
2. Facing the ends with a dremel to prepare flush faced test samples.
3. Cleaning the tube faces with a pick to ensure ends are free of any chips, burrs, or debris.
4. Placing & clamping the tube sample, centered inside of the die, leaving roughly 1.5mm protruding on each side.
5. Flaring the ends to help with crimped-flange formation.
6. Crimping the protruding ends using the linear actuated ram.

GOVERNING EQUATIONS

Bursting Pressure

$$P^* = \frac{2}{\sqrt{3}} K \left[\frac{2}{\sqrt{3}} n\right]^n \frac{t_0}{r_0} \exp(-2n)$$

- ➔ Takes into consideration effects of strain-hardening on deforming material
- ➔ Offers more accurate results over generalized pressure-vessel calculations.

Minimum Forming Pressure

$$P = \frac{2}{\sqrt{3}} K \left[\frac{2}{\sqrt{3}} \left(\ln \frac{r}{r_0}\right)\right]^n t_0 \frac{r_0}{r^2}$$

- ➔ Can be used to determine Forming Loading Curves (FLC) fo complex parts
- ➔ Forming parameters for non-axisymmetric parts like T-Joints can be calculated

BURSTING RESULTS & ANALYSIS

Tube Diameter = 0.1mm

Theoretical Burst Pressure (psi) = 6440	
Average Bursting Pressure = 8140	
Burst Pressure (psi)	Theoretical Error (%)
8100	26
8100	26
8500	32
8000	24
8000	24
Average Error (%) = 26	

Tube Diameter = 0.2mm

Theoretical Burst Pressure (psi) = 12880	
Average Bursting Pressure = 31210	
Burst Pressure (psi)	Theoretical Error (%)
31000	141
31000	141
31000	141
31500	145
32000	148
32050	149
31050	141
31500	145
30000	133
31000	141
Average Error (%) = 142	

CONCLUSIONS & FUTURE WORK

Achievement of the current scope was largely completed. The current system is capable of consistently bursting 2mm OD, stainless steel tubing with wall-thicknesses of both 0.1mm & 0.2mm. This was done with an allocated budget of $500 & several previously acquired components from previous teams working on the micro-THF project.

There are some limitations that were unable to be overcome due to budget & time restrictions:

- Data cannot be stored due to hardware limitations of several components, and must be manually recorded.
- Pressure control is limited due to faulty IP & pressure transducers.
- Actuator control is limited due to lack of a signal wire in the current model.
- Limited actuator control limits the force reading accuracy, causing the sensor to work similarly to an on/off switch.
-

To conclude the semester, the MCHE team is conducting bulge-testing for initial development of an empirical model. Using this initial data, future teams can continue development of an empirical model alongside an analytical model by which forming loading curves can be deduced.

For this to occur, suggestions for modifications to the system to resolve the drawbacks are as follows:

- More accurate force sensor readings, & incremental actuator control through addition of a motor-driver, coded with a pulse-width modulation program.
- Replacement of the IP transducer for incremental control of the output pressure.
- Replacement of the 60k pressure transducer to allow for reading pressures beyond 20kpsi.
- More sophisticated programming & addition of an SD-card slot to allow for data acquisition & storage.

Autonomous Buoy Mesh Network

Team Members: Wyatt Steen (C.), Samuel McBride, Albert McBride, Samantha Linn

Faculty Liaison: Ms. Yasmeen Qudsi

Team Iceberg

Introduction & Background

Competition water skiing courses are comprised of many buoys, held in place with large systems of subsurface systems of cables, piping, and anchors. The American Water Ski Association (AWSA) recognizes three different events and their respective course configurations: slalom, jump, and trick [1]. Construction and maintenance of these courses is time consuming and requires frequent adjustment. A mesh network of autonomous buoys eliminates the need for these systems. This also allows the user to change course configuration remotely.

Figure 1: Course Diagrams

Project Objectives

Goal: Design and develop a scalable and configurable mesh network of autonomous buoys to construct a water ski course.

Objectives:

- Develop a functional design to meet customer requirements and AWSA standards.
- Develop control logic and fabricate a prototype buoy.
- Fabricate and integrate additional buoys to the network.

Materials & Procedure

- A diagram of the buoy is shown in Figure 2.
  - ABS and PVC parts were used for the waterproof housing.
  - Motor mounts and electronics sled were 3D printed in ABS.
  - A steel eyebolt and carabiner are used to fasten the buoy to the subsurface assembly.

Software:

- MATLAB was used to develop control logic of the network.
- XCTU was used to design mesh network architecture using the Zigbee protocol [2].

Hardware:

- The buoy is equipped with an IMU and GPS for pose estimation and navigation.
- An Arduino Micro and XBee RF module are used for processing and communication.
- The system is powered by a 1500mAh LiPo Battery

Fabrication & Analysis

- Housing is constructed of low-cost PVC and ABS parts.
- Custom motor mounts and an electronics sled were 3D printed in ABS.
- Electronics are wired on a prototyping breadboard.

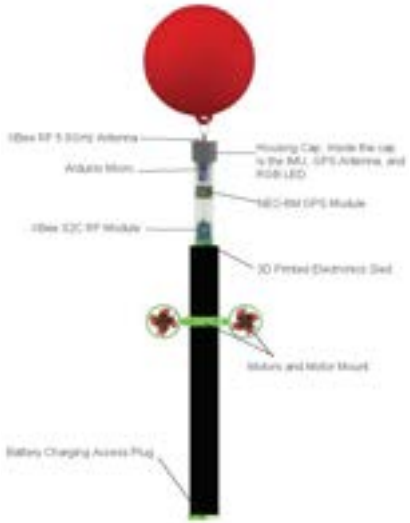

Figure 2: Buoy Diagram

- CFD simulations and buoyancy analyses were conducted in SOLIDWORKS to determine drag and necessary counterweights.

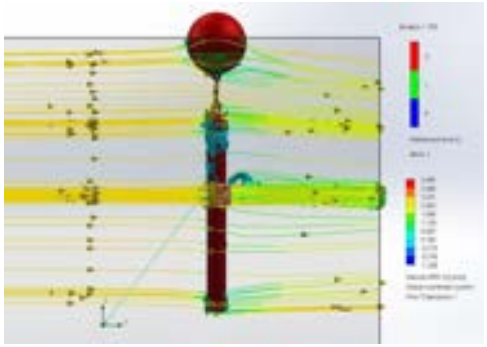

Figure 3: Flow Simulation

Operation & Control

Remote:

- The user has control of the course with a Raspberry Pi based remote.
- The remote is housed in a waterproof case, shown in Figure 4, with is interface mounted on a carbon fiber panel.
- The remote's GUI allows the user to choose desired GPS coordinates of the course, launch and recall the course, as well as modify course configuration and manually adjust course center.

Figure 4: Remote Control GUI

Figure 5: Encased Remote

Conclusion & Future Development

- The manufacture and integration of additional buoys can increase versatility of the network.
- Replacing low-cost sensors with high accuracy sensors can increase performance of the network.
- Electronics systems can be modified to sensors to record performance data of skiers through the course.
- Modification of the housing can adapt the network to several applications beyond water skiing.

References

[1] Official Tournament Rules, USA Water Ski & Wake Sports, Polk City, FL, 2020

[2] "IEEE Standard for Low-Rate Wireless Networks," in *IEEE Std 802.15.4-2015 (Revision of IEEE Std 802.15.4-2011)* , vol., no., pp.1-709, 22 April 2016, doi: 10.1109/IEEESTD.2016.7460875.

Retractor Instrument for Thoracic Surgery

Andrew Hoffpauir, Matthew Matherne, Callie Miller, Tylor Robin, and Yasmeen Qudsi
Department of Mechanical Engineering, University of Louisiana at Lafayette

R.I.T.S.

Keywords: Thoracic Surgery, Retraction, Indication, Compression

Introduction

Surgical procedures are often the last resort to remedy a health condition due to the great risks associated with operations. In thoracic procedures, the ribs are spread open to give access to the chest cavity using a thoracic retractor. The Finochietto retractor, seen in Figure 1, is the most common type of thoracic retractor currently in use. The force a thoracic retractor produces when spreading ribs open can be very large, which can cause harm to the patient, in the form of a broken rib or torn ligaments. Developing a thoracic retractor that can detect the forces produced and even detect tissue damage is important in decreasing the amount of trauma the patient undergoes. The device must be mechanical, easily sterilized, mimic typical thoracic procedures, and cost under $500.

Materials and Methods

- The Spring Block Retractor, shown in Figure 2, is the design utilized to mechanically measure the force during retraction.
- The displacement of the design is directly proportional to the force due to the springs and Hooke's Law, seen in (1).
- The relationship between the displacement of the indication needle versus the force applied to sliding blade is shown in (2), where D_N is the displacement of the tip of the needle and D is the spring displacement
- D_N, calculated in (3), is the total needle displacement
- The retractor instrument underwent compression testing using an MTS machine, shown in Figure 3.

$$F = kd \tag{1}$$

$$D_N = 4\,sin\left[\tan^{-1}\left(\frac{D}{\sqrt{1-D^2}}\right)\right] \tag{2}$$

$$D_N = \begin{cases} 0.875 - 4\sin\left[\tan^{-1}\left(\frac{0.225-D}{\sqrt{1-(0.225-D)^2}}\right)\right] & if\ 0 \le D \le 0.225 \\ 0.875 + 4\sin\left[tan^{-1}\left(\frac{D-0.225}{\sqrt{1-(D-0.225)^2}}\right)\right] & if\ 0.225 \le D \le 0.45 \end{cases} \tag{3}$$

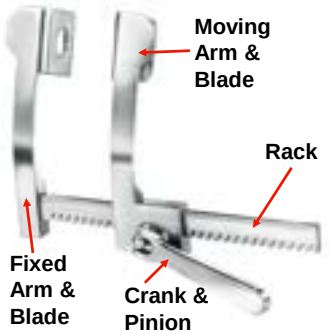

Fig 1: Finochietto Retractor [1]

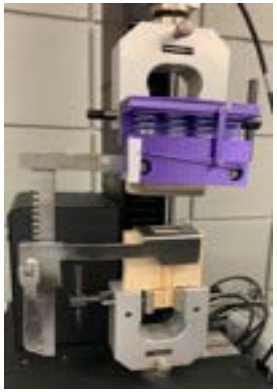

Fig 3: Testing setup on MTS machine

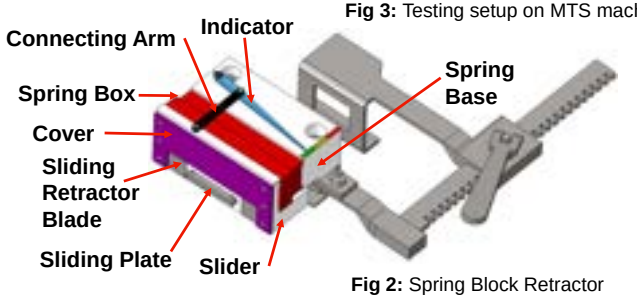

Fig 2: Spring Block Retractor

Spring Constants and Compression Testing

- The stiffness of each spring was tested and is shown in Figure 4.
- Figure 5 shows the theoretical displacement versus the actual displacement of the Spring Block Retractor during testing.
- The Spring Block Retractor was cranked and compared to compression testing. The results, displayed in Figure 6, show the device will measure the same whether applying or reacting to load.

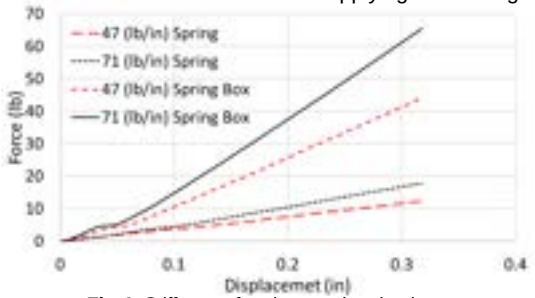

Fig 4: Stiffness of springs and spring boxes

Compression Testing of Spring Block Retractor

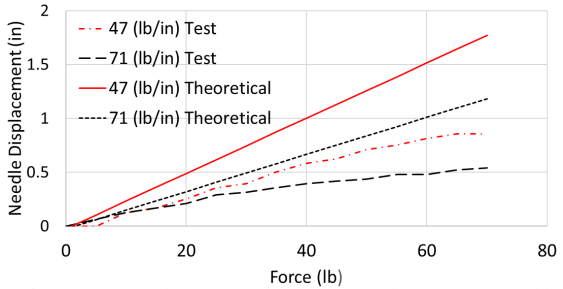

Fig 5: Compression test on the retractor using an MTS machine

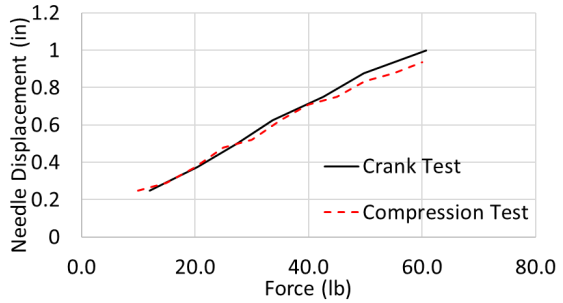

Fig 6: Cranking the retractor versus the MTS machine in compression

Conclusions & Future Work

The Spring Block Retractor was a successful redesign of the surgical instrument to indicate retraction forces during operation. The data collected from the device was linear but did not follow the theoretical data due to friction.

The device can undergo further testing on animal carcasses and human cadavers to determine how it would act in surgical applications. Also, the 3D printed material/parts can be replaced with medical grade materials. The device can also be parameterized so it can be used in patients of all ages and sizes.

References

[1] *"FINOCHIETTO rib spreader." [Online]. Available: https://www.surgiway.com/en/finochietto-rib-spreader-135x38x44-mm-xml-1142_260_466-15605.html.*

UNIVERSITY of LOUISIANA LAFAYETTE | Mechanical Engineering

"A New Look at an Old Decoy"

Team ROJO

Introduction

-The modernized electronic duck decoy lacks innovation, so Team ROJO decided to implement electronic knowledge into a new design.
-Our design incorporates many of the robotic functions seen on the market today into one compact, waterproof, and remotely controllable product.
-Functions include:
- -Jet propulsion
- -Rotating Head
- -Directional Control
- -Realistic Wing Rotation
- -Rippler to disturb water's surface

Methods

-Solidworks used to model all interior mounts and accessories
-3-D printer used to print all mounts and accessories created via Solidworks
-EasyEDA used to custom build Printed Circuit Boards

Outdated Current Market Designs

MOJO:

Rippler:

Revolutionary New Design

Controller Schematic:

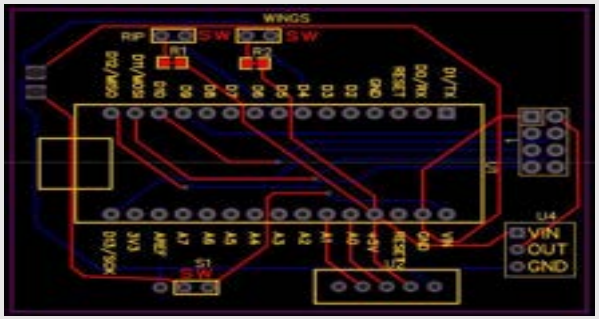

Receiver Schematic:

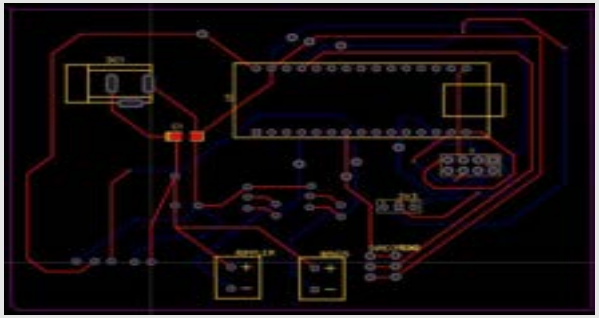

Results

-5 remote functions available
-Waterproof Design
-1 mph max forward propulsion speed
-A realistic wing structure, head, and ripple effect
-2.5 ounces of thrust force
-A rotational speed of 533 RPM for the spinning wings
-A rotational speed of 350 RPM for the rippler
-3lbs 5 ounces with all electronics and mounts involved

Conclusion/Future

-Team ROJO plans on turning the design into a more manufacturable design
-Plan to test the attractiveness to migratory birds this coming duck hunting season

Acknowledgements

-Thanks to Ms. Yasmeen for the circuit troubleshooting
- "I want to buy the first one!!!" –CEO of Acadian Ambulance
- "We want one!!!" – MOJO Outdoors Representative

Team Members

-Jacob Richard
-Conner Hamilton
-Joshua Latiolais
-Tucker Lacombe

Low-Cost Rotating Beam Fatigue Testing System

Caleb Romero, Coby Vincent, Gavin Breaux, Matthew Broussard and Dr. Ayodunde Olayinka
Department of Mechanical Engineering, University of Louisiana at Lafayette

Keywords: Bending Moment , Cycles Until Failure, Fatigue

Introduction

A rotating beam fatigue testing system is a device that uses the rotating beam principle to test the fatigue life of a metal specimen. This device utilizes a ½ horsepower AC motor and a 200lb max force linear actuator to rotate the beam under a load that is beneath its yield stress. In doing so the specimen is constantly being subjected to tension and compression, which after many cycles will cause the specimen to fail. The device will allow the user to set an RPM rate and bending stress, and upon failure will report the number of cycles that the specimen underwent until failure occurred.

Materials and Methods

- 3/16" steel plate was used to create the tabletop, shelf, mounting plates, and magnet housing. A Solidworks FEA analysis was run and proved that the material selection would be sufficient for these applications due to low deflection of the material with the maximum applied loads. Proof can be seen on the right.

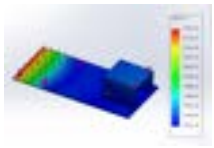

- 1.5"x1.5"x3/16" steel tubing was used to construct the load arm. This beam was designed to handle the maximum load that could be used to test by the machine while maintaining minimum deflection. The FEA analysis can be seen to the right

- 1040 steel rod was used to create an adaptor to connect the load cell to the actuator. This piece was also responsible for being able to withstand the maximum load of testing. The analysis results and proof of material selection can be seen on the right.

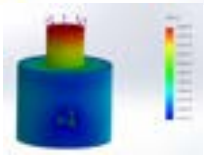

- 1018 cold drawn steel was chosen for the test specimens because of its brittleness, it would allow for shortened testing times. The FEA analysis of a specimen under a 120lb load from the actuator can be seen on the right. These results show how the stress concentration is in the middle of the specimen as assumed.

Component Selection

- A ½ horsepower 3 phase AC motor was selected as the optimal motor choice for controllability, RPM range, and cost effectiveness. This motor allowed for RPM control using a VFD, which allowed the user to vary the speed by varying the frequency of the AC current going to the motor.
- A 200lb maximum force linear actuator was selected to apply the load on the specimen. Since the device was created to test 1018 steel, this actuator's force range more than adequately completed this task.
- Prepacked, low profile, highspeed roller bearings were selected to hold the shafts into position and allowed for easy rotation. The bearings selected can handle speeds of up to 5800 RPM and have a dynamic radial load capacity of 2140lbs.
- 3 couplers were selected. All were 3-piece couplers. The coupler used to connect the motor to the shaft is a 5/8" keyed coupler; the other two are 0.5" couplers, which are utilized as chucks to hold the specimen while testing. The 0.5" couplers were used to reduced vibrations by decreasing runout.
- 5/8" keyed shaft collars were chosen to hold the magnet mounting plate in position on the shaft. They were chosen for ease of assembly and safety.
- 2 Square, zinc yellow-chromate plated steel turntables were selected to act as the pivoting points for the device. They allowed for the device to have all components on the tabletop by allowing the rotation to occur in the horizontal plane.
- 1.25" diameter 0.25" thick circular magnets were selected to work with hall effect sensors to act as a revolution counting mechanism for the device. These magnets have a 1.5lb magnetic force and put out a strong magnetic field for the sensors to detect. These magnets were selected to minimize counting errors.
- 3/8" Ball-point set screws were chosen and used to level the two mounting plates of the device. This was done to limit the vibrations caused by slight slack in the turntables.
- An Arduino based control system was implemented for ease of use. The microcontroller interfaces with the user through the screen, manages the VFD speed and start/stop, controls the actuator, counts the revolutions, and monitors RPM using hall sensors.

Team Spinning Time

Equations of Operation

$$\sigma_{ar} = \frac{32M}{\pi d^3} \quad \text{(Eq. 1)}$$

$$S_e{}' = 0.5 * s_{ut} \quad \text{(Eq. 2)}$$

$$k_a = 2 * S_{ut}^{-0.217} = 2 * 64^{-0.217} = 0.81 \quad \text{(Eq. 3)}$$

$$k_b = 0.879 * d^{-0.107} = 0.879 * 0.3^{-0.107} = 0.9998 \quad \text{(Eq. 4)}$$

$$Se = K_a K_b K_c K_d K_e S_e' \quad \text{(Eq. 5)}$$

$$a = \frac{(f S_{ut})^2}{Se} \quad \text{(Eq. 6)}$$

$$b = -\left(\frac{1}{3}\right) log\left(\frac{f S_{ut}}{Se}\right) \quad \text{(Eq. 7)}$$

$$N = \left(\frac{\sigma_{ar}}{a}\right)^{\frac{1}{b}} \quad \text{(Eq. 8)}$$

Legend of Variables

M Moment

σ_{ar} Alternating stress (completely reversed)

$S_e{}'$ Rotary-beam test specimen endurance limit

k_a Surface factor

k_b Size factor

Se Endurance limit

N Number of cycles to failure

Testing Data

Testing Results of AISI 1018 Steel with 0.3in. Diameter Specimen				
Specimen #	Force applied by load cell (lbs)	RPM (Rev./min.)	Time (s)	Cycles until failure
4	121	2500	190	7916.67
5	120	2500	235	9791.67
6	120	2500	200	8333.33
7	120	2500	297	12375.00
Average	120.25	2500	230.50	9604.17
Standard Deviation			41.87	1744.66

Final Design

Control System Flow Chart

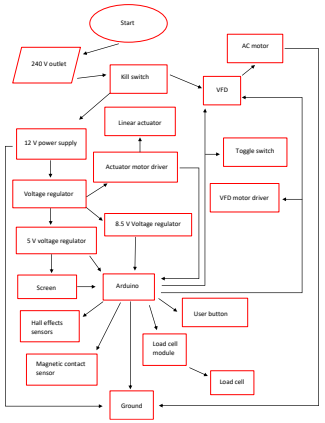

Conclusions & Future Work

The goal of project was to build a fully functional and user-friendly rotating beam fatigue testing system. While this was accomplished, further improvements should be considered to improve the device. It is recommended for future teams to improve the control system and continue to check the integrity of the hardware to ensure that while operating, the device maintains utmost safety. Future teams should also consider the option of switching the clamping mechanism from couplers to collet chucks to decrease the amount of runout across the shafts. Future teams should perform more testing with the device after full calibration to obtain more accurate results as well.

References

- Budynas, R., Nisbett, J. and Shigley, J., n.d. Shigley's Mechanical Engineering Design. 11th ed.

Motorized Micrometer-Driven Aperture System

Alex Tucker, Daylon Thompson, Jake Guidry, John Escoto, Dr. Harry Whitlow, Dr. Jacob King

Background

- The Louisiana Accelerator Center (LAC) is a research lab located on UL south campus
- It houses a 1.7 MV tandem particle accelerator for radiative research experiments
- The accelerator sends an ion beam through a microbeam beam line which is calibrated with an objective and scraper aperture
- Calibration is tedious & time-consuming

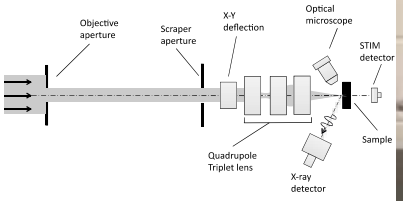

Figure 1: Microbeam Beamline Apparatus [1]

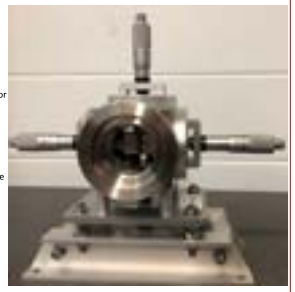

Figure 2: Aperture Housing

Goals

- Reduce the time of the calibration process to increase the window of lab experiments
- Incorporate remote manual control capability at control desk
- Minimum aperture accuracy of 500 nm
- Target aperture accuracy of 100 nm
- Automate the calibration process of setting the area & location of aperture

Design Considerations

- 6 N-cm minimum torque measured to turn micrometer handle
- Design factor of 5 (30 N-cm requirement)
- Micrometer handle rotates & translates
- Gearing backlash
- Ten-year system life
- Minimal change to existing structures

Figure 3: Aperture Dimensions

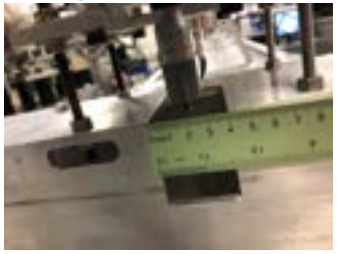

Figure 4: Aperture Dimensions

Proof of Concept

- Single connection to one micrometer handle
- Cost-efficient motors and drivers tested
- Used to prove effectiveness before implementing to all 8 micrometers
- Two iterations:
  1. Friction drive
  2. Direct gearing

Figure 5: Proof of Concept Assembly

Figure 6: SolidWorks Model of Final Design

Summary of Results

- Mechanical drawings and fabrication instructions created
- Mechanical connection between motor & micrometer handle proven effective
- Appropriate motor, driver, power supply, & wiring sizing selected
- Modular prefabricated mounting system selected
- Accuracy of Proof of Concept was between 200 nm and 400 nm (noncumulative error)
- Accuracy can be improved through higher quality motors, drivers, & controllers

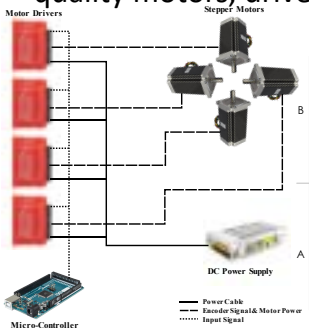

Figure 7: Electrical System Overview

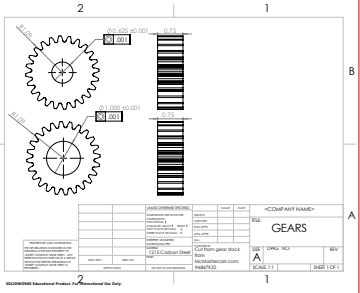

Figure 8: Gear Drawing for Machining

Future Work

- Fabrication & assembly is pending & may be completed the week of May 10, 2021
- Full autonomy can be achieved in the future with the current design

References

[1] Microbeam Focusing: A Laboratory Exercise, Louisiana Accelerator Center., Lafayette, LA, USA, 2020.

Sample Loading and Retrieval System for an Electrostatic Levitation System

Team No Pressure: Jacque Boudreaux, Dylan Derouen, Cullen Jones, Thomas Sapienza, Brennon Bryant
Sponsor: Dr. Jonathan Raush

Introduction

Team No Pressure was assigned with the design and construction of a loading and retrieval system that would improve the overall efficiency of material testing within an Electrostatic Levitation (ESL) system. The new loading design would address the various issues that occurred with the original loading device while also providing a method of retrieving material samples after testing.

Background

Electrostatic levitation (ESL) systems are primarily used to test the thermophysical properties of materials in a container-less environment. The ESL is enclosed in a vacuum chamber to ensure a stable environment while levitating samples. NASA currently uses ESL systems to test and develop new materials for use in space exploration devices.

Improved Design

Volume Reduction:

- 73.5% reduction in air volume over 5 samples
  - Improved Volume = $\left(Volume_{sleeve} + Volume_{reducer} + Volume_{6-way}\right) - Solid\ Volume = 57.45\ in^3$
  - Old Volume = 5 * $\left(\left(Volume_{sleeve} + Volume_{6-way}\right) - Solid\ Volume\right) = 217\ in^3$

Time Reduction:

- Sample-to-Sample time reduced by 93.8%
  - Improved Time = $4 * \left[\left(\frac{Distance_{LA}}{Speed_{LA}}\right) + \left(\frac{Distance_{SA}}{Speed_{SA}}\right)\right] + (2 * Time_{placement}) = 2.63$ minutes
  - Old Time = $\left(4 * \frac{Distance_{Drill}}{Speed_{Drill}}\right) + (Time_{load}) + (2 * Time_{placement}) + Time_{vacuum} = 42.17$ minutes

Other Improvements and features:

- Loads up to 5 samples per pump
- Wireless control from 0-50ft
- Utilizes 2 linear actuators in order to drop samples
  - Large Actuator Velocity = 0.22in/s
  - Small Actuator Velocity = 1.26in/s
- Transfers electricity into the system without breaking vacuum
- Increased sample security
- Easily remove samples after testing using:
  - 6 in OD Funnel
  - 1 in ID Tube
  - 1 in ID Butterfly Valve

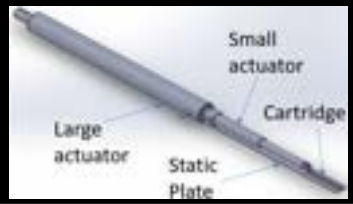

Original Design

Features & Limitations:

- Only loads 1 sample per pump
- Translating motion powered by a drill attached to track system
- Motion control system was very sensitive and inaccurate
- Tongs are used to deliver samples but do not secure samples well
- No method of retrieving the samples after testing

Conclusion

In conclusion the improved design performs about 16 times faster on a sample-to-sample basis. In addition to this the user will have to vacuum out 159.55 in^3 less than when using the old design. These improvements will allow the user to find thermophysical properties inside an ESL system more efficiently. Further analysis can be done on the samples by utilizing the retrieval mechanism.

Future Work

Two areas of the new design presented can be improved to overall increase the functionality of the loading process. First, the control system of the actuators can be reviewed to further increase the efficiency. This could include the installation of sensors or limit switches to improve the accuracy of sample placement to an even higher degree. Lastly, the parts fabricated using manual machining can be remade with a CNC for more effective connections.

Open-Loop Wind Tunnel

Team Wind Tunnel II
Parker Ardoin, Eli Finnegan, Nicholas McMahon, Ian Ransonet
Advisor: Dr. Yonas Niguse

Introduction

An open–loop wind tunnel was asked to be constructed by the University of Louisiana at Lafayette for instructional demonstration and research in the Mechanical Engineering department. The tunnel should include subsystems that will be used to directly measure pressure, temperature, and forces caused by lift and drag. These measurements will be used for further calculations to learn additional information about the properties of airflow in the test section, such as air density, wind velocity, and the coefficient of drag of models.

Fan Selection

McMaster-Carr Model No.	Blade Dia. (in)	Motor Power (HP)	Max. Flow Rate (cfm)
2187K34	20	0.75	6200

Pressure losses accounted for flow velocity, Venturi effect, and flow straightener. These losses can be seen in the equations below.

$$\Delta P_0 = \frac{1}{2}\rho(V_2^2 - V_1^2) \qquad \Delta P_c = \frac{1}{2}\rho K_c V^2 \qquad \Delta P_f = f\frac{l}{2D_H}\rho V^2$$

McMaster-Carr Model 2187K34	Max. Flow Rate (CFM)	Max. Flow Velocity (mph)
Manufacturer's Specs	6200	112.4
Accounting for Pressure Drop	5480	99.3

Mounting System


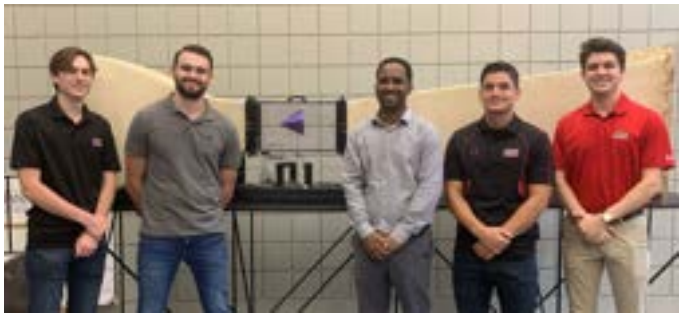

Subassemblies

	Temperature	Pressure	Lift and Drag
Selected Instrument	Type-K Thermocouple	Pitot Tube with Differential Pressure Sensors	Load Cells
Related Equations	$Re = \frac{\rho V l}{\mu}$ $\rho = \frac{P}{RT}$	$P_t = P_s + \frac{\rho V^2}{2}$	$F_x = Kx$
Description	The Type-K Thermocouple allows for a simple way to find flow density, aiding in velocity and Reynold's number calculations.	Using Bernoulli's equation, total and static pressure are related to solve for dynamic pressure. This can then be used to solve for velocity of the flow.	Fixing two load cells, one vertically and one horizontally allows for a simple calculation of lift and drag forces acted upon any model attached to the load cells.


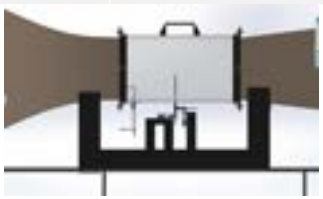

Scale Modeling

For proper scale modeling, three conditions must be met: geometric similarity, kinematic similarity, and dynamic similarity. For testing purposes, basic geometries with known coefficients of drag were used. This allows for an expected force calculation seen in the equation below.

$$F_d = \frac{C_d * A_c * \rho * V^2}{2}$$

Below is a figure showing the coefficients of drag for a few basic geometries.

3D Printed Models




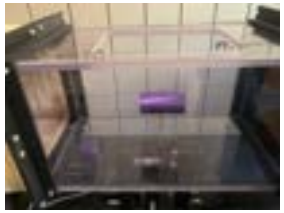

Shake Down Test Results

Thermocouple Test Readings

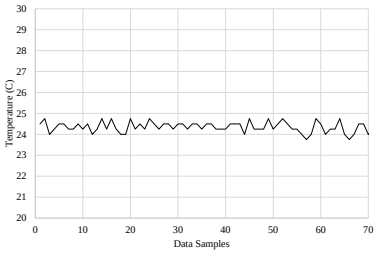

Pressure Sensor Shakedown

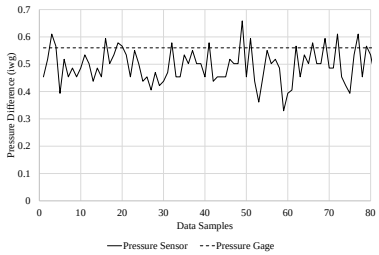

Calculated Velocity Readout

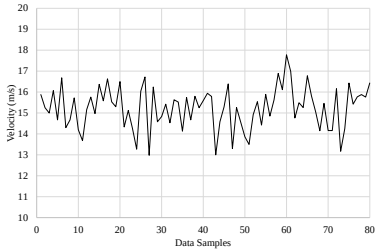

Lift/Downforce Load Cell Shakedown

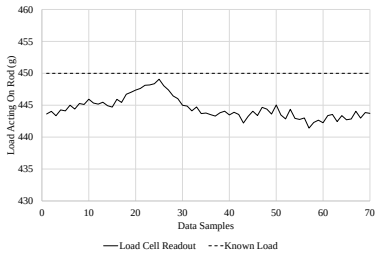

Drag Load Cell Shakedown

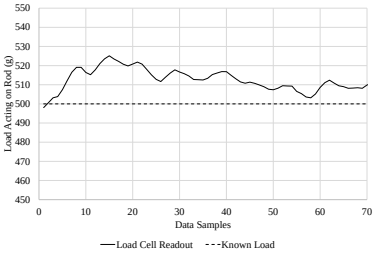

Acknowledgements

Dr. Yonas Niguse
Professor Jeff Guidry
Andrew Hoffpauir

Hart Tools
Gulf Coast Air Systems